Title

Development of thermosensitive resiquimod-loaded liposomes for enhanced cancer immunotherapy.

Authors

Zhang, Hua
Tang, Wei-Lun
Kheirolomoom, Azadeh
et al.

Publication Date

2021-02-01

DOI

10.1016/j.jconrel.2020.11.013

Peer reviewed

Development of thermosensitive resiquimod-loaded liposomes for enhanced cancer immunotherapy

Hua Zhang[a,b,Ψ], **Wei-Lun Tang**[a,Ψ], **Azadeh Kheirolomoom**[a,b], **Brett Z Fite**[a], **Bo Wu**[a], **Kenneth Lau**[a], **Mo Baikoghli**[c], **Marina Nura Raie**[a], **Spencer K. Tumbale**[a], **Josquin Foiret**[a], **Elizabeth S. Ingham**[b], **Lisa M. Mahakian**[b], **Sarah M. Tam**[b], **R. Holland Cheng**[c], **Alexander D. Borowsky**[d], **Katherine W. Ferrara**[e]

[a]Department of Radiology, Stanford University, Palo Alto, CA 94304, USA

[b]Department of Biomedical Engineering, University of California, Davis, CA 95616, USA

[c]Department of Molecular and Cellular Biology, University of California, Davis, CA 95616, USA

[d]Center for Comparative Medicine, University of California, Davis, CA 95616, USA

[e]Molecular Imaging Program, Department of Radiology, Stanford University, 3165 Porter Drive, Palo Alto, CA 94304, USA

Abstract

Resiquimod (R848) is a toll-like receptor 7 and 8 (TLR7/8) agonist with potent antitumor and immunostimulatory activity. However, systemic delivery of R848 is poorly tolerated because of its poor solubility in water and systemic immune activation. In order to address these limitations, we developed an intravenously-injectable formulation with R848 using thermosensitive liposomes (TSLs) as a delivery vehicle. R848 was remotely loaded into TSLs composed of DPPC: DSPC: DSPE-PEG2K (85:10:5, mol%) with 100 mM $FeSO_4$ as the trapping agent inside. The final R848 to lipid ratio of the optimized R848-loaded TSLs (R848-TSLs) was 0.09 (w/w), 10-fold higher than the previously-reported values. R848-TSLs released 80% of R848 within 5 min at 42 °C. These TSLs were then combined with αPD-1, an immune checkpoint inhibitor, and ultrasound-mediated hyperthermia in a *neu* deletion (NDL) mouse mammary carcinoma model (Her2^{+}, ER/PR negative). Combined with αPD-1, local injection of R848-TSLs showed superior efficacy with complete NDL tumor regression in both treated and abscopal sites achieved in 8 of 11 tumor bearing mice over 100 days. Immunohistochemistry confirmed enhanced CD8^{+} T cell infiltration and accumulation by R848-TSLs. Systemic delivery of R848-TSLs, combined with local hyperthermia and αPD-1, inhibited tumor growth and extended median survival from 28 days (non-treatment control) to 94 days. Upon re-challenge with reinjection of tumor cells, none of the previously cured mice developed tumors, as compared with 100% of age-matched control mice.

The dose of R848 (10 μg for intra-tumoral injection or 6 mg/kg for intravenous injection delivered up to 4 times) was well-tolerated without weight loss or organ hypertrophy. In summary, we developed R848-TSLs that can be administered locally or systematically, resulting in tumor regression and enhanced survival when combined with αPD-1 in mouse models of breast cancer.

Graphical Abstract
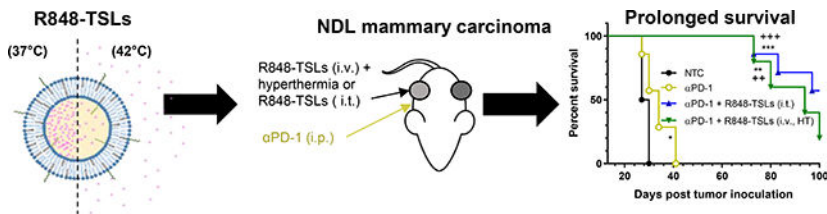
Keywords

Resiquimod; Thermosensitive liposomes; Immunotherapy; Breast cancer; αPD-1

1. Introduction

Breast cancer is the second most common cause of death in women and there are few immunotherapeutic protocols available for advanced or metastatic breast cancer [1]. Recently, the combination of Tecentriq (atezolizumab, PD-L1 check-point inhibitor) and Abraxane (nab-paclitaxel) was the first cancer immunotherapy regimen approved for patients with metastatic triple negative breast cancer who express PD-L1 [2]. In clinical trials, this combination enhanced progression-free survival (PFS), compared to chemotherapy only (combination vs chemotherapy: 7.2 months vs 5.5 months). The clinical result is encouraging and paves the way toward the development of other immunotherapy protocols for metastatic breast cancer.

Toll Like Receptors (TLRs) play a major role in innate immunity by sensing foreign organisms and activating the host defense mechanism against pathogens [3]. Within the past 3 years, 66 clinical trials have begun incorporating TLR agonists [4–6]. While TLR7/8 agonists can be delivered intradermally, the direct delivery of TLR agonists to tumors yields an *in situ* vaccination that improves efficacy by exposing activated immune cells to cancer antigen [7–9]. These studies suggest that prolonged colocalization of antigen and TLR agonist improves antigen presenting cell (APC) co-uptake and therapeutic response [10]. Yet, many of these immunostimulants have poor pharmacokinetic profiles that limit their therapeutic efficacy, even when delivered intratumorally (i.t.) [10, 11]. Used alone [12] or combined with radiotherapy [13–15], chemotherapy [16–19], or other immunotherapeutic reagents [20, 21], TLR7/8 agonists enhanced the immune response in mouse models of lymphoma [17–19, 22, 23], breast cancer [24], gastrointestinal tumor [13], head and neck cancer [20, 25], and pancreatic cancer [12]. When injected systematically or administered orally, the plasma clearance of TLR 7/8 agonists is rapid. Side effects such as systemic inflammation and autoimmune responses have also been observed [26, 27].

To address these issues, TLR7/8 agonists were incorporated into nanoparticles to improve therapeutic efficacy and tumor distribution. In a recent study, resiquimod (R848), a TLR7/8 agonist, encapsulated in β-cyclodextrin nanoparticles facilitated the delivery of R848 to tumor-associated macrophages in vivo and improved immunotherapy response rates when used in combination with an immune checkpoint inhibitor, αPD-1 [28]. Moreover, systemic side effects were reduced [29, 30]. Further, TLR7/8 agonists encapsulated in polymeric nanoparticles were potent immune- adjuvants after subcutaneous injections [31]. Negligible cytotoxicity was observed after local injection of 1 μg of agonist into kidney tumors [31].

Liposomes are safe and effective drug carriers, due to the biocompatibility, drug loading capacity, ease of manufacturing, and potential for activation as well as surface modification [32]. R848-loaded liposomes were previously reported to be efficacious in treating *Leishmanis donovani* infection without significant spleen and liver toxicity [33]. A novel TLR7 agonist, TMX-202, which has a phospholipid moiety, has also been incorporated into liposome membranes [34]. Rarely have TLR agonists been combined with focal therapy. Imiquimod, a TLR7 agonist, formulated with photothermal micellar nanoparticle was highly effective against 4T1 syngeneic murine breast cancer after intravenous injections with a dose of 1.25 mg/kg, particularly when photothermal/immuno-therapy was given in combination with αPD-1 [35]. Here, in order to release the drug within the desired region of interest, thermosensitive liposomes (TSLs) were designed to release the encapsulated drugs rapidly at 42 °C and slowly at body temperature (37 °C) [36]. Most recently, a number of chemotherapeutic drugs have been formulated into TSLs [37, 38] resulting in improved response to treatment as a result of enhanced tumor accumulation and drug release [39]. To the best of our knowledge, TLR agonists have not previously been combined with hyperthermia or ablation and therefore we evaluate this combination therapy. Here, a remote loading technique is used to encapsulate R848 into TSLs with an expected transition temperature of 42 °C (Fig. 1) [37, 38, 40]. Trapping agents are compared and the loading and stability are tuned.

We test R848-TSLs in murine breast tumor models induced through cell injection or allograft tumor transplantation in a multiple implantation model intended as a model of metastasis. While cell injection facilitates quantification of the injected cells and therefore results in consistent tumor growth, allograft tumor transplantation introduces an established tumor microenvironment including immune cells, fibroblasts and endothelial cells. In this paper, we study and compare these models to explore the possible anti-tumor mechanism of R848-TSLs.

Here, in order to create an *in situ* vaccination, we evaluate two schemes for enhanced tumor delivery, local administration to the tumor (after which the drug is slowly released) and systemic administration combined with ultrasound-mediated hyperthermia of the tumor. The optimized R848-TSLs are characterized *in vitro* and *in vivo* in combination with αPD-1 with the goal of achieving a complete response in breast cancer with local release of the agonist by ultrasound-induced hyperthermia.

2. Materials and methods

2.1. Materials

1,2-dipalmitoyl-sn-glycero-3-phosphocholine (DPPC), 1,2-distearoyl-sn-glycero-3-phosphocholine (DSPC), and 1,2-distearoyl-sn-glycero-3-phosphoethanolamine-N-[methoxy(polyethylene glycol)-2000] (ammonium salt) (DSPE-PEG2K) in chloroform were purchased from Avanti Polar Lipids (Alabaster, Alabama). R848 was purchased from Apexbio Technology LLC (Houston, TX). 1,1′-dioctadecyl-3,3,3′,3′-tetramethylindodicarbocyanine (DiD) was purchased from Biotium (Fremont, CA). The *neu* deletion (NDL) metastatic mammary carcinoma cell line was gifted from the Alexander Borowsky Laboratory (UC Davis) [41, 42]. The checkpoint inhibitor, anti-mouse PD-1 antibody (αPD-1) was purchased from Bio X Cell (West Lebanon, NH). Motolimod was purchased from MedChemExpress (Monmouth Junction, NJ). All other reagents were purchased from Sigma-Aldrich, unless otherwise stated.

2.2. Development of R848-TSLs

Liposomes were prepared with a thin-film and rehydration method. First, a lipid thin film was formed by mixing lipids in chloroform in a test tube, with a molar ratio of DPPC: DSPC: DSPE-PEG2K = 80: 15: 5, followed by gentle drying using nitrogen gas and lyophilization for at least two hours. Second, the dried lipid thin film was rehydrated with the trapping agent solution at 58 °C for 30 min, followed with sonication of 15 seconds and extrusion 21 passes through a 100-nm-diameter pore membrane at 55 °C on a mini extruder (Avanti Polar Lipids, Alabaster, AL) to obtain unilamellar liposomes. The medium was exchanged to PBS −/− (without calcium and magnesium, pH 7.4) using a Sephadex G-75 column (GE Healthcare, NJ). The size of the liposomes was measured with a Nano-ZS particle analyzer (Malvern Instruments, Malvern, UK) and the phospholipid concentration was tested with the Phospholipids C kit (Wako Chemicals USA, Inc., VA). The transition temperature (Tm) of the lipids was measured by Differential Scanning Calorimetry (DSC). Unless otherwise specified, R848 (0.2 mg) was added to liposomes with 300 mM trapping agents shown in Table 1, respectively, at an initial R848 to lipid ratio of 1/5 (w/w) followed by 45 min incubation at 37 °C. After drug loading, the liposomes were further purified with Sephadex-G75 columns pre-equilibrated in PBS to remove the unencapsulated R848. The size of the resulting liposomes was measured using a Nano-ZS particle analyzer. The R848 concentration was measured using HPLC-UV, with a standard curve between the UV absorption at 254 nm and injection dose (0–10 μg R848). RP-HPLC was performed using a C4 column (Phenomenex Jupiter 5 μm ID, 250 × 4.6 mm) analytical column with a running gradient with a mixture of Solvent A and Solvent B (Solvent A: water (0.05% v/v trifluoroacetic acid), Solvent B: acetonitrile) from 10 to 60% solvent B in 20 min, followed with a 4 min wash with 90% solvent B and return to 10% solvent B at a flow rate of 1.0 ml/min.

2.3. Cryo-electron microscopy

Cryo-electron microscopy was performed as described previously [40] on a JEOL JEM 2100F operating with a field-emission gun at 200kV. The grid preparation was described previously in [43]. Briefly, 2.5 μL of the solution containing the iron sulfate liposomes (w/

and w/o R848) was placed on Quantifoil R2/2 Cu 300 mesh grids. The grids were pretreated with 20 mAmp of glow discharge for 30 seconds. After one-minute of on-grid incubation, 0.5 μm of NP40 detergent was added for 5 seconds. The excess solution was removed and quickly plunged into liquid ethane using a FEI Vitrobot Mark III semi-automated cryo-plunger. The liposomes were embedded into a thin layer of vitrified ice and transferred into the imaging chamber using a Gatan 626 cryo-transferring system. The grids were examined at 60,000x magnification and images were captured using a D20 direct-electron detector. The digital images were recorded with a pixel size of 0.99 Å using autofocusing scripts in the Serial-EM package, set to a defocus range of 0.5–2.5 nm. The digital images with minimum stigmatism or drift were selected for further statistical analysis and figure preparation.

2.4. Stability of R848-TSLs

A stability study of R848-TSLs in PBS or 50% fetal bovine serum (FBS) was conducted at 37 or 42 °C. R848-TSLs labeled with DiD (1.5% mol) were mixed with heat-deactivated FBS (1:1 v:v) with a final concentration of 250 μg R848/mL, and incubated at 37 °C over a period of 30 min. At the given time points (5, 15, and 30 min), 300 μL of the mixture was collected, and passed through a Sepharose CL-4B column pre-equilibrated with PBS –/– to remove released drugs, and 150 μL of the liposomal fraction was collected. The percentage of drug retention was calculated by the formula, shown below, where [R848] was the concentration of R848 determined by the RP-HPLC method described above. [DiD] was the concentration of DiD as estimated by absorbance at 650 nm by a TECAN microplate reader (Morrisville, NC).

$$R848\ retention\ (\%) = \frac{[R848]_{post\,purification}/[DiD]_{post\,purification}}{[R848]_{t\,=\,0}/[DiD]_{t\,=\,0}} \times 100\%$$

2.5. RAW-Blue activation by R848-TSLs

The TLR activation properties of R848-TSLs and free R848 were quantified with a modified Quanti-Blue™ Assay by measuring the level of secreted embryonic alkaline phosphatase (SEAP) generated by TLR agonist activated RAW-Blue™ macrophages. RAW-Blue macrophages (raw sp, InvivoGen) were maintained according to the manufacturer's instructions in a 37 °C humidified incubator with 5% carbon dioxide with growth medium composed of DMEM (11995, Gibco), 10% heat-inactivated FBS (FB-11, Omega Scientific), 1% Penicillin/Streptomycin (15140, Gibco) and 200 μg/ml of Zeocin™ (ant-zn-1, InvivoGen). RAW-Blue macrophages were plated into a 96-well clear transparent flat bottom tissue culture plate (100,000 cells per well in 100 μL growth medium) and incubated for 24 hrs in a 37 °C humidified incubator with 5% CO_2. The medium was replaced with 100 μL of PBS +/+ (calcium/ magnesium) containing free R848 or R848-TSLs (1:5 serial dilutions from 100 μM to approximately 0.26 nM, in triplicate) and incubated at 37 °C for 5 hrs. After 5 hr incubation, the medium was removed and all samples were washed twice with 100 μL of PBS +/+, then 200 μL test media (same as growth media, except without Zeocin™ selection antibiotic) was added into each well, and the cells were incubated at 37 °C for an additional 24 hrs. After 24 hr incubation, 50 μL of the solution from each well was

transferred into a new 96-well clear transparent flat bottom tissue culture plate containing QUANTI-Blue™ Solution (150 μL per well) and incubated at 37 °C for 3 hrs. After the final incubation, the absorbance at 625 nm was measured with a TECAN microplate reader, and the ratio of the absorbance between treated and untreated cell media was used to characterize TLR activation level.

2.6. Tumor model

All animal experiments were conducted under a protocol approved by the Stanford University or the University of California, Davis, Institutional Animal Care and Use Committee (IACUC). The *Neu* deletion (NDL) mouse model of breast cancer was tested, and in total, 80 bilateral NDL tumor-bearing mice were used in this study. All mice were female FVB mice (6 to 9 weeks old, 20–25 g, Charles River, Wilmington, MA). Mice were orthotopically either transplanted with an NDL tumor fragment (1 mm^3) or injected with NDL cells (1×10^6 cells in 25 μL PBS −/−) into the bilateral #4 and #9 inguinal mammary fat pads [44]. Therapy was started when tumors reached ~4 mm in the largest diameter (approximately 20 days post transplantation or 14 days after cell injections).

2.7. Pharmacokinetic studies

Pharmacokinetic studies were conducted in six female FVB mice: mice were treated by intravenous injections of free R848 or R848-TSLs (n=3 for each group) at a dose of 6 mg/kg, and 150 μL of blood was collected from retro-orbital sinus at selected time points (1, 5, 20 min for free R848, and 1, 20, 60, and 120 min for R848-TSLs) into an EDTA-K3 tube followed by centrifugation at 12,000 rpm for 10 min to obtain the plasma. 50 μL of plasma was spiked with 350 μL cold acetonitrile (0.1% TFA) containing 250 ng/mL motolimod as an internal standard (IS). The mixture was then centrifuged (4 °C) at 20,000g for 10 min. The supernatant was further diluted with MeOH/MeCN (90/10, vol/vol) and centrifuged for another 10 min at 20,000g. 5 μL diluted supernatant was injected on U(H)PLC-MS/MS for quantitative analysis. The U(H)PLC–MS/MS system consists of a ZORBAX sb-c18 HPLC column (4.6 × 150 mm), an Agilent 1290 Infinity Binary Pump, a 1290 Infinity Sampler, and an Agilent Technologies Triple Quad mass spectrometer. A gradient mobile phase was composed of solvent A (Milli-Q water with 0.1% formic acid) and solvent B (acetonitrile with 0.1% formic acid) at a flow rate of 0.3 mL/min with the designed gradient program (0 min, A/B (95/5); 0.8 min, A/B (95/5); 8.5 min, A/B (5/95); 8.6 min, A/B (5/95); 10 min, A/B (95/5)). Detection of R848 and the IS was monitored in ES$^+$ mode using a daughter ion (m/z = 251.2 for R848 and m/z = 330.4 for the IS). All data was acquired using the Agilent Mass Hunter. PK parameters including $t_{1/2}$, C_{max}, and AUC (area under the curve) were obtained by non-compartmental analysis using PKSolver [45].

2.8. Tumor drug retention studies

Nine bilateral NDL bearing mice were studied to determine the drug concentration within the tumors. The mice were randomly assigned to three groups (n=3 each group): free R848 i.t. (10 μg), R848-TSLs i.t. (10 μg), or R848-TSLs i.v. (6 mg/kg) combined with ultrasound-induced hyperthermia (HT). Both treated and distant tumors were harvested 2 hrs post-injection. Harvested tumors were weighed and mixed with cold PBS to obtain 100 mg of tumor/mL followed by 40 sec x 2 homogenization. 50 μL of tumor homogenate was mixed

with 350 μL cold acetonitrile and then centrifuged (4°C) at 20,000g for 10 min. The supernatant was dried and reconstituted with 100 μL MeOH/MeCN (90/10, vol/vol). 5 μL of the reconstituted supernatant was injected for drug analysis with the above-mentioned U(H)PLC-MS/MS system.

2.9. Therapeutic efficacy comparison after short treatments of R848-TSLs alone, R848-TSLs with αPD-1, free R848 with αPD-1, and R848-NTSLs with αPD-1

Twenty cell-injected bilateral tumor mice (4 mm, 11 days after tumor inoculation) were randomly sorted into five groups: 1) non-treatment control (n=3); 2) R848-TSLs (n=4); 3) αPD-1 + R848-TSLs (n=5); 4) αPD-1 + free R848 (n=4); or 5) αPD-1 + R848-NTSLs (n=4). R848-loaded non-temperature sensitive liposomes (R848-NTSLs) was prepared based on the previous preparation method [46]. Liposomal or free R848 were injected i.t. (10 μg in 17 μl of PBS each injection) into one tumor twice per week with two treatments in total, and αPD-1 was injected i.p. (200 μg in 50 μl of PBS each injection) once per week with one injection in total. One week after the first treatments, tumors were harvested for immnunohistochemistry.

2.10. Therapeutic efficacy comparison between extended treatment with R848-TSLs and free R848, each combined with αPD-1

Sixteen transplantation bilateral tumor mice (4 mm, 21 days after tumor inoculation) were randomly sorted into three groups: 1) non-treatment control (n=5); 2) αPD-1 + free R848 (n=4); or 3) αPD-1 + R848-TSLs (n=7). Liposomal or free R848 were injected i.t. (10 μg in 50 μL of PBS each injection) into one tumor twice per week with four treatments in total, and αPD-1 was injected i.p. (200 μg in 50 μL of PBS each injection) once per week with three injections in total. Tumors were measured with an ultrasound system (Siemens Acuson Sequoia C512, DE) and the tumor size (mm^3) was calculated with the following equation:

$$\text{Tumor volume (mm}^3) = \frac{a * b * c}{6} \pi$$

Where a, b, and c are the lengths (mm) of the major, minor, or vertical axis, respectively. The tumor growth was calculated with the following equation, where the V is the tumor volume:

$$\text{Tumor growth (\%)} = \left(V - V_{Day0}\right)/V_{Day0} * 100$$

2.11. Survival studies

Survival studies were performed with both transplanted and cell-injection bilateral tumor mice, as listed in Table 2.

R848-TSLs were administered either i.t. (10 μg R848 in 50 μL of PBS each injection) or intravenously (6 mg/kg) twice a week with four treatments in total, and αPD-1 was injected intraperitoneally (200 μg in 50 μL of PBS −/− each injection) once per week with three injections in total. Mice were euthanized when either the tumor size limit was reached (the

combination of the largest dimension of all the lesions reach 17.5 mm), or when ulceration was detected.

2.12. Hyperthermia

For the mice treated with hyperthermia, one tumor from each mouse was treated with hyperthermia to trigger the local release and the contralateral tumor served as a control. The tumor insonation was started 5 min prior to administration of R848-TSLs at 42 °C, and continued for an additional 20 min post injection. Image-guided hyperthermia was performed using a programmable ultrasound system (Vantage 256, Verasonics, Kirkland, WA) with a setup developed for activatable delivery of nanoparticles [40, 47]. Tumor heating was generated with a custom 128-element 1.5 MHz therapeutic array designed for rodents [48]. Heating was performed with ultrasound bursts of 1.8 MPa peak negative pressure, with a pulse repetition frequency of 100 Hz and burst duration ranging from 0 to 8 ms as controlled by a proportional integral derivative (PID) controller (duty cycle ranging from 0 to 0.8) set to maintain the core tumor temperature at 42 °C. A hypodermic needle thermocouple (HYP1–30-1/2-T-G-60-SMP-M, Omega Engineering) provided the temperature feedback for the PID controller.

2.13. Tumor re-challenge

Mice cured from the previous NDL transplantation (n=4) or cell injection (n=4) studies were re-challenged by injecting 1×10^6 NDL cells into the untreated side fat pad, and age-matched naive mice (n=4) were used as control. Tumor size and body weight were monitored and euthanization was performed with the criteria described above in Section 2.11.

2.14. Histological analysis

Tissues for microscopic analysis were fixed overnight in 20% buffered formalin and transferred to 70% ethanol the next day. A Tissue-Tek VIP autoprocessor (Sakura, Torrance, CA) was used to process samples for paraffin-embedding. Tissue blocks were then sectioned to 4 μm, sections mounted on glass slides. Hematoxylin and Eosin (H&E) staining was performed at the University of California, Davis, Dept. of Pathology and Laboratory Medicine. Immune cells were stained with specific antibodies based on the manufacturer's instructions. Anti-mouse CD8 (1:500 dilution; 14–0808, eBiosciences) was used as CD8 marker. Anti-mouse CD68 (1:700 dilution; PA1518, Boster) was used to stain macrophages. Anti-mouse OX40 antibody (1:2000 dilution; ab229021, abcam) was used to label the activated T cells. Anti-mouse CD206 (1:2000 dilution; ab64693, abcam) was used as a marker for M2 macrophages. Detection of the primary antibodies was performed using the appropriate isotype specific species secondary antibody with the Vectastain ABC Kit Elite Kit and a diaminobenzidine Peroxidase Substrate Kit (Vector Labs, Burlingame, CA) for amplification and visualization of signal. Stained slides were scanned on an AT2 Scanscope (Leica Biosystems), and digital images viewed using the Imagescope software.

2.15. Statistical analysis

Statistical analyses were performed using Prism 8 software (GraphPad Software Inc.). Results are presented as mean ± SEM unless otherwise indicated. For analysis of 3 or more

groups, a one-way ANOVA test was performed followed by a Tukey's multiple comparison correction in GraphPad Prism. Analysis of differences between 2 normally distributed test groups was performed using an unpaired t-test assuming unequal variance. P values less than 0.05 were considered significant.

3. Results

3.1. Optimization of R848 loading in thermosensitive liposomes

R848 was remotely loaded into the TSLs with trapping agents (Table 1) under the same incubation conditions (37 °C for 45 min) with an R848 to lipid ratio of 1/5 (w/w). The loading capacity was greatest with 300 mM $FeSO_4$ among the trapping agents tested, including copper sulfate, ammonium sulfate, ammonium citrate, and aluminum sulfate (Fig. 2A). To decrease the membrane stress caused by hyper-osmolarity inside the liposomes and therefore enhance stability [49, 50], we studied loading R848 with a lower $FeSO_4$ concentration. The reduction of $FeSO_4$ concentration from 300 to 100 mM decreased the loading efficiency from 0.13 ± 0.01 to 0.09 ± 0.01 mg/mg (Fig. 2B); however, the resulting mass of drug was found to be sufficient for efficacy in early studies (not shown). Therefore, R848-encapsulated liposomes with 100 mM $FeSO_4$ were used to conduct the *in vitro* and *in vivo* studies described in this study.

3.2. Characterization of R848-TSLs

As shown in Table 3, loading R848 into thermosensitive liposomes with 100 mM $FeSO_4$ did not significantly change the liposome size and zeta potential as compared to the empty liposome. The resulting R848-TSLs have an average diameter of 110.3 ± 19.8 nm with narrow polydispersity index (PDI) < 0.05. Liposomal size was monitored up to 3 weeks at 4 °C and the size and PDI were unchanged over this period. The final drug to lipid ratio of R848-TSLs was 0.09 (w/w) with ~50% R848 encapsulation.

Iron oxide precipitation was evident near the inner leaflet of the bilayer membrane on cryo-EM images of R848-TSLs, but was not detected in empty liposomes (Fig. 2 C and D). Morphology and zeta potential of the loaded and empty liposomes were similar, with an average size of ~110 nm. However, the standard deviation of the mean diameter on light scattering and cryoEM micrographs were greater for empty liposomes.

3.3. Suitability of R848-TSLs for triggered drug release

In the *in vitro* stability study (Fig. 2E), drug release from R848-TSLs was 12% over 30 min in PBS at 37 °C. However, in 50% serum, 60% of the drug was released in the first 5 min and the remaining drug (~40%) was retained in the liposomes over 30 min at 37 °C. At 42 °C, rapid drug release (~80%) occurred within 5 min, which was consistent with the transition temperature (Tm: 43.12 °C) of R848-TSLs, as confirmed by DSC (Fig. S1). The results indicate that R848-TSLs are thermosensitive and drug release can be triggered in response to mild hyperthermia (42 °C).

3.4. RAW-Blue™ macrophage activation by R848-TSLs

We verified that the R848-TSLs retained potency in the activation of RAW-Blue™ macrophages. As shown in Fig. 2F, a slightly lower EC_{50} concentration was required for R848-TSLs to induce NF-κB activity in RAW-Blue™ macrophages than free R848 (19.6 vs 68.9 nM).

3.5. In vivo pharmacokinetics of free R848 and R848-TSLs after intravenous injection

R848-TSLs increased the drug half-life by 2.5 fold, the area under the curve (AUC) by 22 fold, and C_{max} by 9 fold, compared to free R848, as shown in Fig. 2G and Table 4.

3.6. R848-TSLs retain drug 2h after intra-tumoral injection or intra-tumoral release of drug

Two hours post intra-tumoral injection of 10 μg free R848 or R848-TSLs, the concentration of R848 in R848-TSL injected tumors was 37 fold higher than achieved with the direct i.t. injection of free R848, and the distant tumor concentration was 19 fold higher when R848-TSLs were injected as compared with free drug (Fig. 2H). For local injection of R848-TSLs and free R848, the local concentration was 20 and 39 fold higher than the distant tumor concentration, respectively, suggesting that in each case the drug was absorbed into the vasculature.

We also evaluated the injection of 6 mg/kg (~120 μg for a 20 g mouse) of R848-TSLs i.v. coupled with release by ultrasound hyperthermia. Here, the tumor drug concentration was 3 times higher in the insonified tumor as compared with the contralateral, suggesting that a fraction of the drug remained sequestered. With this protocol, the intratumoral drug concentration achieved was similar to that resulting from direct i.t. free drug administration and the concentration in the distant tumor was similar to that resulting from direct i.t. injection of R848-TSLs.

3.7. Local injection of R848-TSLs, in combination with systemic injection of αPD-1, increases CD8+ T cells and macrophages

To study the mechanism of the R848-TSL treatment, we compared the tumor histology after treatments with R848 (free, in non-temperature sensitive liposomes (NTSLs), or in TSLs), with or without αPD-1 (Fig. 3). CD8+ T cell density with (R848-TSLs + αPD-1) treatment was significantly higher than the non-treatment control (NTC), (free R848 + αPD-1) and (R848-NTSLs + αPD-1), while OX40+ T cell density after (R848-TSLs + αPD-1) treatment was significantly higher than (R848-TSLs alone). R848-TSLs combined with αPD-1 significantly increased CD68+ macrophage density, while the CD206+ macrophages (marking the M2 polarized subset) did not change significantly with either R848-TSLs alone or (R848-TSLs + αPD-1), indicating an increase in CD68+/CD206− macrophages.

3.8. Local injection of R848-TSLs results in complete tumor regression of treated and distant transplanted NDL tumors

To evaluate the antitumor efficacy of R848-TSLs, we first compared i.t. injection of R848-TSLs vs free R848, each combined with αPD-1 treatment. (Fig. 4A). αPD-1 alone did not

result in significant tumor regression, as compared with the non-treatment control (Fig. 4B, C). Tumor regression was faster and more consistent with R848-TSL treatment as compared with free R848 (Fig. 4 B–E). Eleven of twelve tumors (including treated and distant) regressed after the first or second dose of R848-TSLs, and the 12th tumor regressed on the third dose. The majority of tumors (5 of 8) treated with free R848 required three or more doses, with one tumor not responding after the 4th dose (Fig. 4 G, H). The area under the curve (AUC) of tumor growth was therefore reduced by the R848-TSL treatment as compared with free R848 (p = 0.021) (Fig. 4F).

3.9. αPD-1 combined with R848-TSLs increased T cells infiltration in both treated and distant tumors and improved antitumor activity

A majority of the treated and distant tumors completely regressed after 4 i.t. administrations of R848-TSLs (combined with αPD-1) within a 1-week period. Most tumors were not detected by ultrasound or optical inspection after necropsy. Immunohistochemistry was performed on the tumors that did not regress completely. Low or no detectable viability was observed on H&E staining compared with the NTC (pink vs purple color in the H&E images, Fig. 5A, D, G and magnified Fig. 5B, E, H). CD8$^+$ T cell infiltration was enhanced in both treated and distant tumors in the R848-TSL cohort (Fig. 5C, F, I, J).

3.10. Efficacy study

3.10.1. Local injection of R848-TSLs eradicated all transplanted NDL tumors
—We first assessed efficacy in a model of tumor transplantation, as we have observed that such models are particularly advantageous for cancer immunotherapy due to the reduction in the fibrosis and immune response frequently seen with cell-injected tumors. With the treatment regimen depicted in Fig. 4A (4 intra-tumoral injections of R848-TSLs and 3 i.p. injections of αPD-1), tumors started to regress after the second treatment, similar to the results in Fig. 4 (Fig. 6 A–D), while αPD-1 treatments alone did not slow tumor growth (Fig. 6A–B). When combined with αPD-1, all R848-TSL treated and distant tumors regressed completely before or on Day 42 post tumor inoculation (24 days after the first treatment), and tumor recurrence was not observed. Tumor growth required humane euthanasia in the control cohorts (no-treatment control, or αPD-1 group) within 38 days after tumor inoculation (Fig. 6 A, B, E). No body weight loss was observed during or after treatment with the combination therapy or αPD-1 only (Fig. 6F). Individual tumor volume and growth plots are detailed in Fig. 6G–N.

3.10.2. Local injection of R848-TSLs resulted in a complete response in the majority of mice with cell-injected tumors—We next assessed both i.t. and i.v. injections of R848-TSLs in a cell injection model using the treatment regimen presented in Fig. 7A. Reduced tumor growth and volume and enhanced survival was demonstrated for the combined treatments without loss of body weight (Fig. 7B–S). In the R848-TSL (i.t.) treatment group (Fig. 7 J, P), all treated tumors regressed after the first injection and 6 of 7 continued to regress after the second or third injection. Tumors were eradicated before or on Day 45 post tumor inoculation (or 32 days after the first treatment), and ~ 50% of treated tumors (4 of 7) did not recur within 150 days. Most of the distant tumors (5 of 6) regressed completely by Day 45 after tumor inoculation and 4 of them did not return (Fig. 7K, Q).

For the tumors treated with R848-TSLs i.v. + HT (Fig. 7 L, R), all (5 of 5) regressed within 24 days after the first treatment (Day 37 after tumor inoculation) and most were too small to be detected. However, most of the treated tumors (4 of 5) returned 2–6 weeks later, with slow tumor growth observed over the following 30 to 50 days. Tumor regrowth was also observed in 4 of 5 distant tumors (Fig. 7 M, S). The median survival of NTC, αPD-1, (αPD-1 + R848-TSLs i.t.), and (αPD-1 + R848-TSLs i.v. + HT) cohorts was 28.5, 34, greater than 100, and 94 days, respectively.

In summary, both i.t. and i.v. plus HT treatments of R848-TSLs, combined with αPD-1, delayed tumor growth where i.t. treatment eradicated both treated and distant tumors (Fig. 7 B–E). Compared to the no-treatment control or αPD-1 cohorts, both R848-TSLs treatments prolonged the survival of NDL tumor bearing mice (Fig. 7F).

3.10.3.   αPD-1 combined with R848-TSLs generated systemic tumor-specific immunity against NDL—To understand whether a specific adaptive immune response could be generated by our proposed combination therapy (αPD-1 + R848-TSLs i.t.), we re-challenged the mice cured from the efficacy studies (NDL cell injection & NDL transplantation) by injecting NDL cells into the untreated side fat pad at 153 days after the first tumor inoculation. After tumor re-challenge, zero of eight R848-TSL-treated mice grew tumors at 100 days (the longest observed time). In contrast, all mice from an age-matched control group developed tumors upon inoculation and were euthanized by 60 days post re-challenge due to tumor volume (Fig. 8).

4.   Discussion

In this paper, we set out to evaluate the efficacy of immunotherapeutics with delivery strategies that concentrate the dose in the tumor microenvironment, yet efficiently release the contents. We evaluated two approaches: directly injecting the R848-TSLs in the tumor and injecting R848-TSLs systemically and releasing the drug in the tumor. We compared these approaches with the injection of free drug and the injection of long-circulating liposomes in a subset of studies. We added αPD-1 as our previous work has shown that CD8^{+} T cells in this model express PD-1 (immune checkpoint) and efficacy is enhanced with the addition of αPD-1. Our central goal in this study was to demonstrate that the two approaches of interest each result in a rapid and sustained regression. The rate and reproducibility of the response was superior for these approaches as compared with the injection of free drug.

At the dose of 10 μg per i.t. injection (40 μg in total dose in the entire treatment regimen), R848-TSLs induced a slightly faster and more consistent response in both treated and distant tumors than free R848. One possible explanation for the enhanced effect is that liposomes increase the tumor retention of R848 [51], as evidenced by the 37 fold higher R848 concentration in the R848-TSL-treated vs free R848-treated tumors. R848-TSLs retain the same biological activity and induced TLR activation in RAW-Blue™ macrophages in a manner similar to free R848. This cell line expresses all TLRs (except for TLR5) and therefore provides a good environment for the assessment of TLR agonists. When tested in PBS +/+, R848-TSLs induced TLR activation at a slightly faster rate (a slightly lower EC50 than free R848). This may result from enhanced cellular uptake by endocytosis as shown in

Supplementary Information Figure S3, which facilitates the delivery of R848 to TLR 7 and 8 on the endosomal membrane [52].

TLR agonist treatments have been reported to generate long-term immunological memory, protecting animals against specific tumor re-challenge [14, 15, 18, 20, 22, 28, 53–60]. However, most small TLR 7/8 agonists such as resiquimod (R848) are poorly water soluble, resulting in limited therapeutic efficacy and drug delivery [61]. In recent studies, R848 was encapsulated into conventional liposomes, composed of saturated lipids and cholesterols with a transition temperature above 55 °C, by passive or remote loading to improve drug delivery as well as its solubility [33, 62]. However, loading via passive techniques results in low loading efficiency. When ammonium sulfate was used as a drug trapping agent, loading was increased five-fold, yet the formulation stability was limited. Here, we used $FeSO_4$ as a trapping agent to improve loading.

While we chose to study R848 here, many agonists can be similarly loaded and locally delivered in future studies. To the best of our knowledge, this is the first reported study of a temperature-sensitive liposomal formulation for R848. In a long-term survival study, i.t. injections of R848-TSLs cured 9 of 11 NDL mice and tumors did not develop on re-challenge. No significant body weight loss or irregular behavior was observed during or after the treatment regimen, demonstrating that the combination therapy was safe to use. Therefore, we believe TSL-mediated delivery of immunotherapy agents can be an effective and safe approach to advance agonist cancer immunotherapy.

Combined with high frequency ultrasound or hyperthermia, TSLs have been frequently utilized to assist the locally effective release of chemotherapeutics such as doxorubicin in solid tumors with significantly improved therapeutic outcomes in preclinical and clinical studies [63, 64]. Heat-triggered delivery of drug overcomes dependence on passive extravasation of drug-carrying nanoparticles through the enhanced permeation and retention (EPR) effect [65]. Most importantly, such vehicles deliver large fractions of the injected dose. For a human tumor with a 2 cm radius, 5% blood volume, 10 second blood transit time and 5 L full blood volume, the fraction of the injected dose delivered is ~ 8% for 40 minutes of heating. This is orders of magnitude greater than the dose delivered to human tumors by any other systemic method, which is typically 0.01% of systemically-injected drug [37, 40, 47, 66–69]. Therefore, ultrasound mediated local release of R848 from TSLs was explored here to amplify the local immune response without unwanted systemic side effects.

4.1 Tumor model

We also observed differences in efficacy between NDL cell-injection and transplantation tumor models. Tumors induced by NDL cell injection grew faster than transplanted tumors (13 vs 18 days to reach 4mm in diameter) and were less responsive to R848-TSLs i.t. treatment (57% vs 100% survival over the course of 100 days, respectively). While the cell-injected tumors contain only tumor cells, transplanted tumors include tumor cells, fibroblasts, and immune cells. We hypothesize that the resident immune cells within the transplanted tumors may enhance immunotherapeutic response. Given that the transplanted tumors more closely mimic the human breast cancer [70], the complete response of the

transplanted NDL tumors treated with i.t. injections of R848-TSLs (100% survival and no tumor growth upon re-challenge) is encouraging.

4.2 Loading and stability

To improve loading, we first optimized the trapping agent. Among these tested trapping agents, we found that 300 mM $FeSO_4$ achieved the highest drug encapsulation (13%, w/w) and the result was significantly higher than previously reported values of 1.1% by passive loading [33, 62] or 4.4% by active loading [62], where conventional liposomes were used. In contrast to conventional liposomes with a high transition temperature (> 55 °C), TSLs are composed of low transition temperature lipids (~41 °C, slightly higher than the body temperature) and are relatively fluidic and less stable. It is therefore more difficult to encapsulate and retain hydrophobic drugs such as R848. With our drug loading approach, R848 can be efficiently encapsulated into TSLs with improved formulation stability (< 15% drug leakage in 30 min at 37 °C in PBS) and higher drug encapsulation than previously reported [51]. In order to reduce the membrane stress caused by hyperosmolarity of 300 mM $FeSO_4$, a lower concentration of $FeSO_4$ was ultimately tested for loading R848, and we found that 100 mM $FeSO_4$ could load 0.09 (w/w) R848.

During drug loading, the color of the liposome-R848 mixture turned brown from light blue, indicating iron ions were directly or indirectly involved in R848 encapsulation. Fe precipitation was observed on cryo-EM of R848-TSLs in the vicinity of lipid membranes. One possible reason for this observation is the oxidation of Fe^{2+} to Fe^{3+} by the elevated pH during the R848 loading, resulting in the formation of insoluble $Fe(OH)_3$ precipitates. Previous cryo-EM studies of TSLs containing doxorubicin [37], gemcitabine [40], and other hydrophobic drugs [71–73] reported higher electron density and crystallization inside liposomes. Here, this was not observed. For $CuSO_4$, the trapping agent with the 2nd highest R848 loading tested here, lowering the concentration from 300 to 100 mM caused a 3 times decrease of the R848 loading (0.09 vs 0.03 w/w, data not shown). We also tested 100 mM copper gluconate with triethanolamine (pH 8.4), which was used as the trapping agent for doxorubicin [37] and gemcitabine [74] TSLs. As compared with doxorubicin or gemcitabine, the combination of copper gluconate and triethanolamine (pH 8.4) loaded R848 at a drug to lipid ratio of 0.01, far lower than that achieved with $FeSO_4$ (0.09 mg/mg). This indicates the internal pH might also affect the loading efficiency in addition to drug-metal complexation or metal precipitation. Also, iron ions seem to have higher affinity to R848 than copper ions as evidenced by UV absorption enhancement with increasing iron concentrations in Fig. S2, and better stabilize encapsulated R848 and minimize the drug leakage from TSLs. Less than 10% drug release was observed at 4 °C in 1 month (data not shown) and less than 15% of drug release was detected at 37 °C for 30 min. However, 60% burst release was detected from R848-TSLs when incubated in 50% serum at 37 °C within the first 5 min, suggesting that R848 might reside partially at the inner liposomal membrane (easier to release) and partially inside the liposomes (more stable). The membrane association was also suggested by our cryo-EM results. Nevertheless, R848-TSLs release more than 90% of the cargo in serum with mild hyperthermia (40–43 °C), indicating the drug release is heat-triggerable.

4.3 Anti-tumor mechanism of R848-TSLs

Resiquimod, a TLR7/8 agonist, has direct anti-tumor efficacy through both myeloid differentiation primary-response 88 (MYD88) dependent or MYD88-independent pathways. For details of the direct anti-tumor molecular mechanisms of R848, please refer to [75, 76]. In the study reported here, R848-TSLs did not significantly reduce NDL and RAW-blue macrophage growth at the concentration found within the tumors (Supplementary Information Fig. S4). At 2hr post intra-tumoral injections of R848-TSLs, the R848 concentration decreased to 3.8 μg/g, which is significantly below the EC50.

Compared with free R848, R848-TSLs increased tumor accumulation over 37 fold (Fig. 2H), increased the infiltration of CD8^{+} T cells (Fig. 3C), and increased the rate and reduced the variance in tumor growth (Fig. 4F). We also observed that R848-TSLs were efficiently internalized by RAW-blue macrophages through clathrin-mediated endocytosis, as chlorpromazine blocked clathrin-mediated endocytosis (Supplementary Information Fig. S3). This provides a second potential mechanism for enhanced intracellular delivery and efficacy.

The combination of R848-TSLs with αPD-1 increased OX40 expression and CD68^{+}/CD206^{-} macrophages. Similar to [28, 77, 78], we found that R848-TSLs combined with αPD-1 increased the non-M2 macrophage population.

4.4 Limitations of the study

A minimum set of controls was explored given the complexity: 2 administration routes (IV with ultrasound vs IT injection) for 3 formulations (free drug, TSLs, non-temperature sensitive liposomes), with and without αPD-1, two tumor models. There are clearly many additional controls and studies that can be pursued in the future.

Many preclinical and clinical studies have suggested that the route of administration can impact the therapeutic efficacy of TLR agonists [79], and understanding these effects is crucial to the success of liposomal R848 development. In the cell injection model, few immune cells are present within the tumor at the start of treatment. In the tumor transplant model, a full tumor microenvironment is quickly established. With cell-injected NDL tumors, the injection route (i.t. or i.v.) impacted the treatment outcome. The fraction of mice that exhibited rebound tumor progression increased from 18% with i.t injection (10 μg per injection) to 100% with i.v. injection (120 μg per injection) + HT at 60 days post-treatment. This increase in tumor rebound rate likely results from the lower local drug availability resulting from instability of R848-TSLs in systemic circulation. Despite the improved *in vivo* half-life of R848-TSLs (2.5 fold longer) in our current formulation the delivered dose may be insufficient [80] in some models.

Future studies will be focused on improving the serum stability of R848-TSLs. In addition, the effective tumor R848 i.v. dose delivered by TSLs, and the interaction between R848-TSLs and immune cells will be studied further to maximize the therapeutic efficacy of the combination of HIFU and R848.

5. Conclusions

We developed a thermosensitive liposome formulation with high drug payload for local and systemic delivery of R848. Despite moderate drug release in 50% serum, local delivery of the R848-TSLs combined with αPD-1 treatment can effectively eradicate NDL transplanted tumors (both treated and distant tumors) via enhanced tumor infiltration of CD8^{+} T cells with no recurrence over 100 days with 100% survival (4 out of 4). In a more aggressive tumor model developed by tumor cell injection rather than transplantation, i.t. injection of R848-TSLs regressed all treated and distant tumors, and 4 out of 7 were tumor free over 100 days. R848-TSLs injected i.v. combined with local hyperthermia and αPD-1 increased the median survival by ~3 fold when compared with non-treatment control or αPD-1 treatment only. All of the tumor-free mice from the local delivery of the R848-TSLs combined with αPD-1 treatment developed specific immunity against NDL cells, and did not grow tumor after NDL tumor re-challenge. Together, R848-TSLs combined with αPD-1 could be a promising therapeutic strategy for enhanced cancer immunotherapy.

Supplementary Material

Refer to Web version on PubMed Central for supplementary material.

Acknowledgements

Abbreviations

APC	antigen-presenting cells
AUC	area under curve
DiD	1,1′-dioctadecyl-3,3,3′,3′- tetramethylindodicarbocyanine
DPPC	1,2-dipalmitoyl-sn-glycero-3-phosphocholine
DSPC	1,2-distearoyl-sn-glycero-3-phosphocholine
DSC	Differential Scanning Calorimetry
DSPE-PEG2K	1,2-distearoyl-sn-glycero-3-phosphoethanolamine-N-[methoxy(polyethylene glycol)-2000] (ammonium salt)
HPLC	high-performance liquid chromatography
HT	hyperthermia
i.t.	intratumoral
i.v.	intravenous
i.p.	intraperitoneal

NDL	*neu* deletion (mouse breast tumor model)
NTSL	non-temperature sensitive liposomes
PBS	phosphate buffered saline
PDI	polydispersity index
R848	resiquimod
TLR	Toll-like Receptor
Tm	melting temperature
TSL	Thermosensitive liposomes
UV	ultra-violet

Reference

[1]. Cancer.Net, Breast Cancer https://www.cancer.net/, 2020.

[2]. FDA approves atezolizumab for PD-L1 positive unresectable locally advanced or metastatic triple-negative breast cancer., (2019).

[3]. Barton GM, Medzhitov R, Toll-like receptors and their ligands, Current topics in microbiology and immunology 270 (2002) 81–92. [PubMed: 12467245]

[4]. Sabado RL, Pavlick A, Gnjatic S, Cruz CM, Vengco I, Hasan F, Spadaccia M, Darvishian F, Chiriboga L, Holman RM, Escalon J, Muren C, Escano C, Yepes E, Sharpe D, Vasilakos JP, Rolnitzsky L, Goldberg JD, Mandeli J, Adams S, Jungbluth A, Pan L, Venhaus R, Ott PA, Bhardwaj N, Resiquimod as an Immunologic Adjuvant for NY-ESO-1 Protein Vaccination in Patients with High-Risk Melanoma, Cancer Immunology Research 3(3) (2015) 278–287. [PubMed: 25633712]

[5]. Kang J, Demaria S, Formenti S, Current clinical trials testing the combination of immunotherapy with radiotherapy, Journal for ImmunoTherapy of Cancer 4(1) (2016).

[6]. Smith M, Garcia-Martinez E, Pitter MR, Fucikova J, Spisek R, Zitvogel L, Kroemer G, Galluzzi L, Trial Watch: Toll-like receptor agonists in cancer immunotherapy, Oncoimmunology 7(12) (2018).

[7]. Frank MJ, Reagan PM, Bartlett NL, Gordon LI, Friedberg JW, Czerwinski DK, Long SR, Hoppe RT, Janssen R, Candia AF, Coffman RL, Levy R, In Situ Vaccination with a TLR9 Agonist and Local Low-Dose Radiation Induces Systemic Responses in Untreated Indolent Lymphoma, Cancer Discovery 8(10) (2018) 1258–1269. [PubMed: 30154192]

[8]. Sagiv-Barfi I, Czerwinski DK, Levy S, Alam IS, Mayer AT, Gambhir SS, Levy R, Eradication of spontaneous malignancy by local immunotherapy, Sci Transl Med 10(426) (2018).

[9]. Sagiv-Barfi I, Kohrt HE, Burckhardt L, Czerwinski DK, Levy R, Ibrutinib enhances the antitumor immune response induced by intratumoral injection of a TLR9 ligand in mouse lymphoma, Blood 125(13) (2015) 2079–2086. [PubMed: 25662332]

[10]. Tomai MA VJ, Chapter 8 - Toll-Like Receptor 7 and 8 Agonists for Vaccine Adjuvant Use., in: Press A (Ed.), Immunopotentiators in Modern Vaccines (Second Edition)2017, pp. 149–162.

[11]. TY W, Strategies for designing synthetic immune agonists, Immunology 148 (2016) 315–325. [PubMed: 27213842]

[12]. Michaelis KA, Norgard MA, Zhu XX, Levasseur PR, Sivagnanam S, Liudahl SM, Burfeind KG, Olson B, Pelz KR, Ramos DMA, Maurer HC, Olive KP, Coussens LM, Morgan TK, Marks DL, The TLR7/8 agonist R848 remodels tumor and host responses to promote survival in pancreatic cancer, Nat. Commun. 10 (2019) 15. [PubMed: 30604768]

[13]. Schölch S, Rauber C, Tietz A, Rahbari NN, Bork U, Schmidt T, Kahlert C, Haberkorn U, Tomai MA, Lipson KE, Carretero R, Weitz J, Koch M, Huber PE, Radiotherapy combined with TLR7/8

activation induces strong immune responses against gastrointestinal tumors, Oncotarget 6(7) (2015) 4663–4676. [PubMed: 25609199]

[14]. Dovedi SJ, Adlard AL, Ota Y, Murata M, Sugaru E, Koga-Yamakawa E, Eguchi K, Hirose Y, Yamamoto S, Umehara H, Honeychurch J, Cheadle EJ, Hughes G, Jewsbury PJ, Wilkinson RW, Stratford IJ, Illidge TM, Intravenous administration of the selective toll-like receptor 7 agonist DSR-29133 leads to anti-tumor efficacy in murine solid tumor models which can be potentiated by combination with fractionated radiotherapy, Oncotarget 7(13) (2016) 17035–17046. [PubMed: 26959743]

[15]. Herrera FG, Bourhis J, Coukos G, Radiotherapy combination opportunities leveraging immunity for the next oncology practice, CA-Cancer J. Clin. 67(1) (2017) 65–85. [PubMed: 27570942]

[16]. Kasturi SP, Skountzou I, Albrecht RA, Koutsonanos D, Hua T, Nakaya HI, Ravindran R, Stewart S, Alam M, Kwissa M, Villinger F, Murthy N, Steel J, Jacob J, Hogan RJ, Garcia-Sastre A, Compans R, Pulendran B, Programming the magnitude and persistence of antibody responses with innate immunity, Nature 470(7335) (2011) 543–7. [PubMed: 21350488]

[17]. Zhu J, He S, Du J, Wang Z, Li W, Chen X, Jiang W, Zheng D, Jin G, Local administration of a novel Toll-like receptor 7 agonist in combination with doxorubicin induces durable tumouricidal effects in a murine model of T cell lymphoma, Journal of Hematology and Oncology 8(1) (2015) 1–10. [PubMed: 25622682]

[18]. Cheadle EJ, Lipowska-Bhalla G, Dovedi SJ, Fagnano E, Klein C, Honeychurch J, Illidge TM, A TLR7 agonist enhances the antitumor efficacy of obinutuzumab in murine lymphoma models via NK cells and CD4 T cells, Leukemia 31(7) (2017) 1611–1621. [PubMed: 27890931]

[19]. Gao D, Li W, Wang W, Cai Y, Wang Y, Luo X, Wei CC, Synergy of purine-scaffold TLR7 agonist with doxorubicin on systemic inhibition of lymphoma in mouse model, Journal of Cancer 8(16) (2017) 3183–3189. [PubMed: 29158790]

[20]. Sato-Kaneko F, Yao S, Ahmadi A, Zhang SS, Hosoya T, Kaneda MM, Varner JA, Pu M, Messer KS, Guiducci C, Coffman RL, Kitaura K, Matsutani T, Suzuki R, Carson DA, Hayashi T, Cohen EEW, Combination immunotherapy with TLR agonists and checkpoint inhibitors suppresses head and neck cancer, JCI Insight 2(18) (2017) 1–18.

[21]. Lynn GM, Sedlik C, Baharom F, Zhu YL, Ramirez-Valdez RA, Coble VL, Tobin K, Nichols SR, Itzkowitz Y, Zaidi N, Gammon JM, Blobel NJ, Denizeau J, de la Rochere P, Francica BJ, Decker B, Maciejewski M, Cheung J, Yamane H, Smelkinson MG, Francica JR, Laga R, Bernstock JD, Seymour LW, Drake CG, Jewell CM, Lantz O, Piaggio E, Ishizuka AS, Seder RA, Peptide-TLR-7/8a conjugate vaccines chemically programmed for nanoparticle self-assembly enhance CD8 T-cell immunity to tumor antigens, Nat. Biotechnol. (2020) 19.

[22]. Dovedi SJ, Melis MHM, Wilkinson RW, Adlard AL, Stratford IJ, Honeychurch J, Illidge TM, Systemic delivery of a TLR7 agonist in combination with radiation primes durable antitumor immune responses in mouse models of lymphoma, Blood 121(2) (2013) 251–259. [PubMed: 23086756]

[23]. Wiedemann GM, Jacobi SJ, Chaloupka M, Krächan A, Hamm S, Strobl S, Baumgartner R, Rothenfusser S, Duewell P, Endres S, Kobold S, A novel TLR7 agonist reverses NK cell anergy and cures RMA-S lymphoma-bearing mice, OncoImmunology 5(7) (2016) 1–11.

[24]. Yin T, He S, Wang Y, Toll-like receptor 7/8 agonist, R848, exhibits antitumoral effects in a breast cancer model, Mol Med Rep 12(3) (2015) 3515–3520. [PubMed: 26043701]

[25]. Lu RL, Groer C, Kleindl PA, Moulder KR, Huang A, Hunt JR, Cai S, Aires DJ, Berkland C, Forrest ML, Formulation and preclinical evaluation of a toll-like receptor 7/8 agonist as an anti-tumoral immunomodulator, J. Control. Release 306 (2019) 165–176. [PubMed: 31173789]

[26]. Pockros PJ, Guyader D, Patton H, Tong MJ, Wright T, McHutchison JG, Meng TC, Oral resiquimod in chronic HCV infection: Safety and efficacy in 2 placebo-controlled, double-blind phase IIa studies, J. Hepatol. 47(2) (2007) 174–182. [PubMed: 17532523]

[27]. Savage P, Horton V, Moore J, Owens M, Witt P, Gore ME, A phase I clinical trial of imiquimod, anoral interferon inducer, administered daily, Br. J. Cancer 74(9) (1996) 1482–1486. [PubMed: 8912549]

[28]. Rodell CB, Arlauckas SP, Cuccarese MF, Garris CS, Li R, Ahmed MS, Kohler RH, Pittet MJ, Weissleder R, TLR7/8-agonist-loaded nanoparticles promote the polarization of tumour-

associated macrophages to enhance cancer immunotherapy, Nature Biomedical Engineering 2(8) (2018) 578–588.

[29]. Shi JJ, Kantoff PW, Wooster R, Farokhzad OC, Cancer nanomedicine: progress, challenges and opportunities, Nat. Rev. Cancer 17(1) (2017) 20–37. [PubMed: 27834398]

[30]. Kamaly N, Yameen B, Wu J, Farokhzad OC, Degradable Controlled-Release Polymers and Polymeric Nanoparticles: Mechanisms of Controlling Drug Release, Chem. Rev. 116(4) (2016) 2602–2663. [PubMed: 26854975]

[31]. Kim H, Niu L, Larson P, Kucaba TA, Murphy KA, James BR, Ferguson DM, Griffith TS, Panyam J, Polymeric nanoparticles encapsulating novel TLR7/8 agonists as immunostimulatory adjuvants for enhanced cancer immunotherapy, Biomaterials 164 (2018) 38–53. [PubMed: 29482062]

[32]. Allen TM, Cullis PR, Liposomal drug delivery systems: From concept to clinical applications, Adv. Drug Deliv. Rev. 65(1) (2013) 36–48. [PubMed: 23036225]

[33]. Peine KJ, Gupta G, Brackman DJ, Papenfuss TL, Ainslie KM, Satoskar AR, Bachelder EM, Liposomal resiquimod for the treatment of Leishmania donovani infection, J Antimicrob Chemother 69(1) (2014) 168–75. [PubMed: 23956375]

[34]. Klauber TCB, Laursen JM, Zucker D, Brix S, Jensen SS, Andresen TL, Delivery of TLR7 agonist to monocytes and dendritic cells by DCIR targeted liposomes induces robust production of anti-cancer cytokines, Acta Biomaterialia 53 (2017) 367–377. [PubMed: 28153581]

[35]. Zhang L, Jing D, Wang L, Sun Y, Li JJ, Hill B, Yang F, Li Y, Lam KS, Unique Photochemo-Immuno-Nanoplatform against Orthotopic Xenograft Oral Cancer and Metastatic Syngeneic Breast Cancer, Nano Letters 18(11) (2018) 7092–7103. [PubMed: 30339018]

[36]. Ganta S, Devalapally H, Shahiwala A, Amiji M, A review of stimuli-responsive nanocarriers for drug and gene delivery, J. Control. Release 126(3) (2008) 187–204. [PubMed: 18261822]

[37]. Kheirolomoom A, Lai CY, Tam SM, Mahakian LM, Ingham ES, Watson KD, Ferrara KW, Complete regression of local cancer using temperature-sensitive liposomes combined with ultrasound-mediated hyperthermia, J. Control. Release 172(1) (2013) 266–273. [PubMed: 23994755]

[38]. Kheirolomoom A, Mahakian LM, Lai CY, Lindfors HA, Seo JW, Paoli EE, Watson KD, Haynam EM, Ingham ES, Xing L, Cheng RH, Borowsky AD, Cardiff RD, Ferrara KW, Copper-Doxorubicin as a Nanoparticle Cargo Retains Efficacy with Minimal Toxicity, Mol. Pharm. 7(6) (2010) 1948–1958. [PubMed: 20925429]

[39]. Nardecchia S, Sanchez-Moreno P, de Vicente J, Marchal JA, Boulaiz H, Clinical Trials of Thermosensitive Nanomaterials: An Overview, Nanomaterials 9(2) (2019).

[40]. Tucci ST, Kheirolomoom A, Ingham ES, Mahakian LM, Tam SM, Foiret J, Hubbard NE, Borowsky AD, Baikoghli M, Cheng RH, Ferrara KW, Tumor-specific delivery of gemcitabine with activatable liposomes, J. Control. Release 309 (2019) 277–288. [PubMed: 31301340]

[41]. Miller JK, Shattuck DL, Ingalla EQ, Yen LL, Borowsky AD, Young LJT, Cardiff RD, Carraway KL, Sweeney C, Suppression of the Negative Regulator LRIG1 Contributes to ErbB2 Overexpression in Breast Cancer, Cancer Res. 68(20) (2008) 8286–8294. [PubMed: 18922900]

[42]. Siegel PM, Ryan ED, Cardiff RD, Muller WJ, Elevated expression of activated forms of Neu/ErbB-2 and ErbB-3 are involved in the induction of mammary tumors in transgenic mice: implications for human breast cancer, Embo J. 18(8) (1999) 2149–2164. [PubMed: 10205169]

[43]. Xing L, Li TC, Mayazaki N, Simon MN, Wall JS, Moore M, Wang CY, Takeda N, Wakita T, Miyamura T, Cheng RH, Structure of Hepatitis E Virion-sized Particle Reveals an RNA-dependent Viral Assembly Pathway, J. Biol. Chem. 285(43) (2010) 33175–33183. [PubMed: 20720013]

[44]. Borowsky AD, Namba R, Young LJT, Hunter KW, Hodgson JG, Tepper CG, McGoldrick ET, Muller WJ, Cardiff R, Gregg JP, Syngeneic mouse mammary carcinoma cell lines: Two closely related cell lines with divergent metastatic behavior, Clin. Exp. Metastasis 22(1) (2005) 47–58. [PubMed: 16132578]

[45]. Zhang Y, Huo MR, Zhou JP, Xie SF, PKSolver: An add-in program for pharmacokinetic and pharmacodynamic data analysis in Microsoft Excel, Comput. Meth. Programs Biomed. 99(3) (2010) 306–314.

[46]. Tang W-L, Tang W-H, Chen WC, Diako C, Ross CF, Li S-D, Development of a Rapidly Dissolvable Oral Pediatric Formulation for Mefloquine Using Liposomes, Mol. Pharm. 14(6) (2017) 1969–1979. [PubMed: 28460165]

[47]. Kheirolomoom A, Silvestrini MT, Ingham ES, Mahakian LM, Tam SM, Tumbale SK, Foiret J, Hubbard NE, Borowsky AD, Ferrara KW, Combining activatable nanodelivery with immunotherapy in a murine breast cancer model, J Control Release 303 (2019) 42–54. [PubMed: 30978432]

[48]. Liu J, Foiret J, Stephens DN, Le Baron O, Ferrara KW, Development of a spherically focused phased array transducer for ultrasonic image-guided hyperthermia, Phys Med Biol 61(14) (2016) 5275–5296. [PubMed: 27353347]

[49]. Hallett FR, Marsh J, Nickel BG, Wood JM, Mechanical-Properties of Vesicles. 2. A model for osmotic swelling and lysis, Biophys. J. 64(2) (1993) 435–442. [PubMed: 8457669]

[50]. Hupfeld S, Moen HH, Ausbacher D, Haas H, Brandl M, Liposome fractionation and size analysis by asymmetrical flow field-flow fractionation/multi-angle light scattering: influence of ionic strength and osmotic pressure of the carrier liquid, Chem. Phys. Lipids 163(2) (2010) 141–147. [PubMed: 19900428]

[51]. Maeda H, Nakamura H, Fang J, The EPR effect for macromolecular drug delivery to solid tumors: Improvement of tumor uptake, lowering of systemic toxicity, and distinct tumor imaging in vivo, Adv. Drug Deliv. Rev. 65(1) (2013) 71–79. [PubMed: 23088862]

[52]. Petes C, Odoardi N, Gee K, The Toll for Trafficking: Toll-Like Receptor 7 Delivery to the Endosome, Front Immunol 8 (2017) 1075–1075. [PubMed: 28928743]

[53]. Holldack J, Toll-like receptors as therapeutic targets for cancer, Drug Discov Today 19(4) (2014) 379–82. [PubMed: 24012797]

[54]. Bocanegra Gondan AI, Ruiz-de-Angulo A, Zabaleta A, Gómez Blanco N, Cobaleda-Siles BM, García-Granda MJ, Padro D, Llop J, Arnaiz B, Gato M, Escors D, Mareque-Rivas JC, Effective cancer immunotherapy in mice by polyIC-imiquimod complexes and engineered magnetic nanoparticles, Biomaterials 170 (2018) 95–115. [PubMed: 29656235]

[55]. Sagiv-Barfi I, Czerwinski DK, Levy S, Alam IS, Mayer AT, Gambhir SS, Levy R, Eradication of spontaneous malignancy by local immunotherapy, Sci. Transl. Med. 10(426) (2018) 12.

[56]. Zaharoff DA, Hance KW, Rogers CJ, Schlom J, Greiner JW, Intratumoral Immunotherapy of Established Solid Tumors With Chitosan/IL-12, J. Immunother. 33(7) (2010) 697–705. [PubMed: 20664357]

[57]. Dovedi SJ, Lipowska-Bhalla G, Beers SA, Cheadle EJ, Mu L, Glennie MJ, Illidge TM, Honeychurch J, Antitumor Efficacy of Radiation plus Immunotherapy Depends upon Dendritic Cell Activation of Effector CD8+ T Cells, Cancer Immunology Research 4(7) (2016) 621–630. [PubMed: 27241845]

[58]. Ito H, Combination therapy with TLR7 agonist and radiation is effective for the treatment of solid cancer, Annals of Translational Medicine 4(5) (2016) 5–7. [PubMed: 26855941]

[59]. Park CG, Hartl CA, Schmid D, Carmona EM, Kim HJ, Goldberg MS, Extended release of perioperative immunotherapy prevents tumor recurrence and eliminates metastases, Sci. Transl. Med. 10(433) (2018) 14.

[60]. Sallets A, Robinson S, Kardosh A, Levy R, Enhancing immunotherapy of STING agonist for lymphoma in preclinical models, Blood Adv. 2(17) (2018) 2230–2241. [PubMed: 30194137]

[61]. Chi H, Li C, Zhao FS, Zhang L, Ng TB, Jin G, Sha O, Anti-tumor Activity of Toll-Like Receptor 7 Agonists, Front Pharmacol 8 (2017) 304–304. [PubMed: 28620298]

[62]. Duong AD, Collier MA, Bachelder EM, Wyslouzil BE, Ainslie KM, One Step Encapsulation of Small Molecule Drugs in Liposomes via Electrospray-Remote Loading, Mol. Pharm. 13(1) (2016) 92–99. [PubMed: 26568143]

[63]. Nardecchia S, Sánchez-Moreno P, Vicente J.d., Marchal JA, Boulaiz H, Clinical Trials of Thermosensitive Nanomaterials: An Overview, Nanomaterials (Basel) 9(2) (2019) 191.

[64]. Kneidl B, Peller M, Winter G, Lindner LH, Hossann M, Thermosensitive liposomal drug delivery systems: state of the art review, Int J Nanomedicine 9 (2014) 4387–4398. [PubMed: 25258529]

[65]. Kobayashi H, Watanabe R, Choyke PL, Improving Conventional Enhanced Permeability and Retention (EPR) Effects; What Is the Appropriate Target?, Theranostics 4(1) (2014) 81–89.

[66]. Al Basha S, Salkho N, Dalibalta S, Hussein GA, Liposomes in Active, Passive and AcousticallyTriggered Drug Delivery, Mini-Reviews in Medicinal Chemistry 19(12) (2019) 961–969. [PubMed: 30961495]

[67]. Gray MD, Lyon PC, Mannaris C, Folkes LK, Stratford M, Campo L, Chung DYF, Scott S, Anderson M, Goldin R, Carlisle R, Wu F, Middleton MR, Gleeson FV, Coussios CC, Focused Ultrasound Hyperthermia for Targeted Drug Release from Thermosensitive Liposomes: Results from a Phase I Trial, Radiology 291(1) (2019) 232–238. [PubMed: 30644817]

[68]. Yang C, Li Y, Du M, Chen Z, Recent advances in ultrasound-triggered therapy, Journal of Drug Targeting 27(1) (2019) 33–50. [PubMed: 29659307]

[69]. Kheirolomoom A, Ingham ES, Mahakian LM, Tam SM, Silvestrini MT, Tumbale SK, Foiret J, Hubbard NE, Borowsky AD, Murphy WJ, Ferrara KW, CpG expedites regression of local and systemic tumors when combined with activatable nanodelivery, J Control Release 220(Pt A) (2015) 253–264. [PubMed: 26471394]

[70]. Mollard S, Mousseau Y, Baaj Y, Richard L, Cook-Moreau J, Monteil J, Funalot B, Sturtz FG, How can grafted breast cancer models be optimized?, Cancer Biol. Ther. 12(10) (2011) 855–864. [PubMed: 22057217]

[71]. Tang WL, Tang WH, Szeitz A, Kulkarni J, Cullis P, Li SD, Systemic study of solvent-assisted active loading of gambogic acid into liposomes and its formulation optimization for improved delivery, Biomaterials 166 (2018) 13–26. [PubMed: 29529479]

[72]. Tang WL, Tang WH, Chen WC, Diako C, Ross CF, Li SD, Development of a Rapidly Dissolvable Oral Pediatric Formulation for Mefloquine Using Liposomes, Mol. Pharm. 14(6) (2017) 1969–1979. [PubMed: 28460165]

[73]. Tang WL, Chen WC, Roy A, Undzys E, Li SD, A Simple and Improved Active Loading Method to Efficiently Encapsulate Staurosporine into Lipid-Based Nanoparticles for Enhanced Therapy of Multidrug Resistant Cancer, Pharm. Res. 33(5) (2016) 1104–1114. [PubMed: 26758590]

[74]. Tucci ST, Kheirolomoom A, Ingham ES, Mahakian LM, Tam SM, Foiret J, Hubbard NE, Borowsky AD, Baikoghli M, Cheng RH, Ferrara KW, Tumor-specific delivery of gemcitabine with activatable liposomes, J Control Release (2019).

[75]. Chi H, Li C, Zhao FS, Zhang L, Ng TB, Jin G, Sha O, Anti-tumor activity of toll-like receptor 7 agonists, Frontiers in Pharmacology 8(MAY) (2017) 1–10. [PubMed: 28149278]

[76]. Dowling DJ, Recent Advances in the Discovery and Delivery of TLR7/8 Agonists as Vaccine Adjuvants, ImmunoHorizons 2(6) (2018) 185–197. [PubMed: 31022686]

[77]. Thauvin C, Widmer J, Mottas I, Hocevar S, Alleman E, Bourquin C, Delie F, Development of resiquimod-loaded modified PLA-based nanoparticles for cancer immunotherapy: A kinetic study, Eur. J. Pharm. Biopharm. 139 (2019) 253–261. [PubMed: 30981947]

[78]. Schmid D, Park CG, Hartl CA, Subedi N, Cartwright AN, Puerto RB, Zheng YR, Maiarana J, Freeman GJ, Wucherpfennig KW, Irvine DJ, Goldberg MS, T cell-targeting nanoparticles focus delivery of immunotherapy to improve antitumor immunity, Nat. Commun. 8 (2017) 12. [PubMed: 28400552]

[79]. Engel AL, Holt GE, Lu H, The pharmacokinetics of Toll-like receptor agonists and the impact on the immune system, Expert Rev Clin Pharmacol 4(2) (2011) 275–289. [PubMed: 21643519]

[80]. Spinetti T, Spagnuolo L, Mottas I, Secondini C, Treinies M, Rüegg C, Hotz C, Bourquin C, TLR7-based cancer immunotherapy decreases intratumoral myeloid-derived suppressor cells and blocks their immunosuppressive function, OncoImmunology 5(11) (2016) e1230578. [PubMed: 27999739]

Highlights:

- Iron sulfate (100 mM) was used to trap poorly water-soluble resiquimod (R848) in thermosensitive liposomes (R848-TSLs).

- The R848 to lipid ratio of R848-TSLs could reach 0.09 (w/w).

- > 80% of the encapsulated drug was released from R848-TSLs within 5 min at 42–43 °C.

- Infiltrating CD8$^+$ T cells in *neu* deletion mouse breast tumors increased after treatment with R848-TSLs and αPD-1.

- Superior tumor regression, long-term survival, and specific tumor immunity memory were achieved with of R848-TSLs and αPD-1.
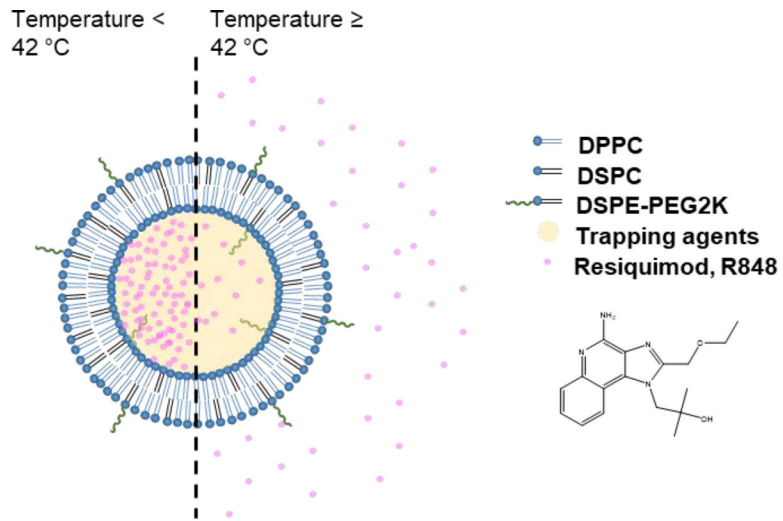
Figure 1.
Scheme for triggered release of R848 from R848-TSLs with mild hyperthermia (42 °C).
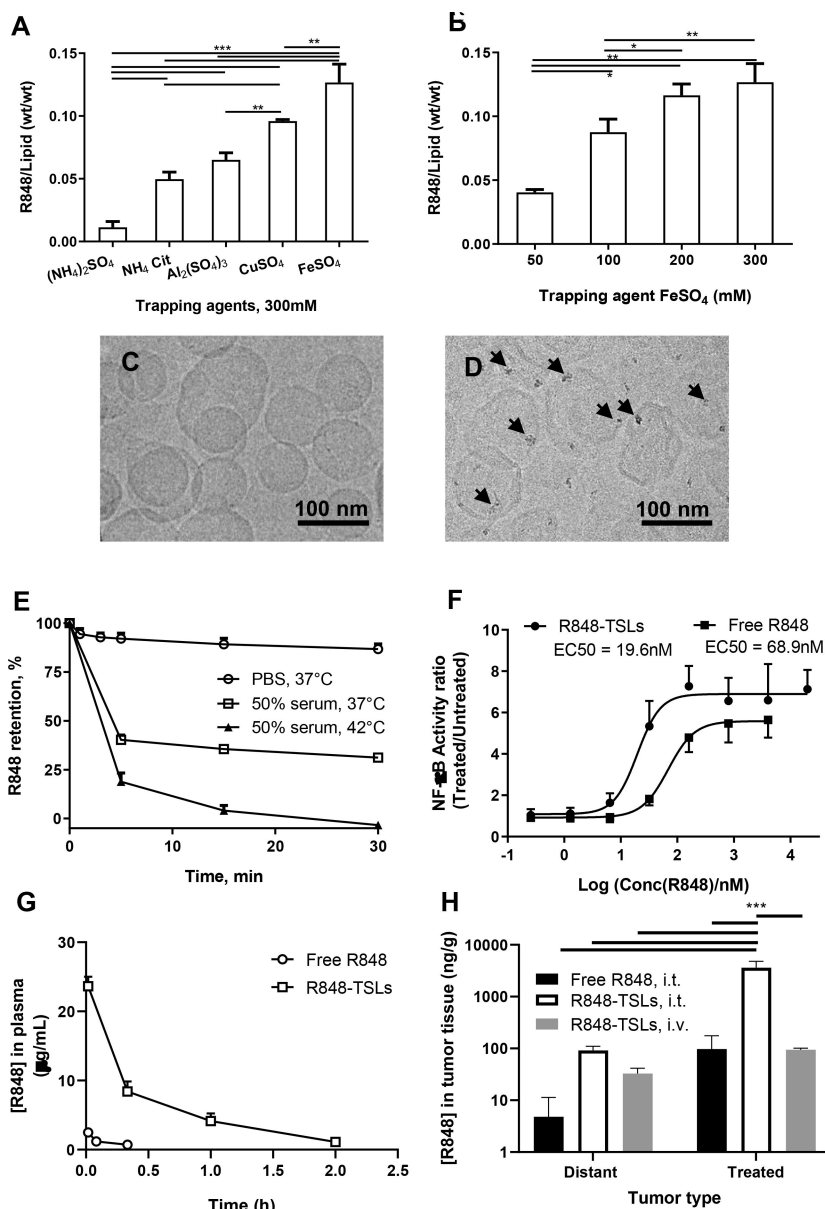
Figure 2.

Optimization of R848 loading in TSLs and characterization of R848-TSLs. A) Effect of various trapping agents on R848 loading. B) Effect of $FeSO_4$ concentration on the drug loading; C) and D) cryo-EM images of TSLs before (C) and after (D) R848 loading, where the black arrows point to iron-R848 co-precipitate. E) Stability of R848-TSLs in PBS at 37 °C, in 50% serum at 37 °or 42 °C. F) NF-κB activation by R848-TSLs in RAW-Blue™ macrophages. Data = mean ± SD ($n = 3$). G) *In vivo* pharmacokinetics of free R848 and R848-TSLs after i.v. injection. H) Tumor concentration of R848 (log scale) 2hrs after intra-tumoral injection of free R848 or R848-TSLs, or after i.v. injections of R848-TSLs. One-way ANOVA applied for A, B. Two-way ANOVA applied to H. * $p<0.05$; **$p<0.01$; ***$p<0.001$. (For interpretation of the references to color in this figure legend, the reader is referred to the web version of this article.)
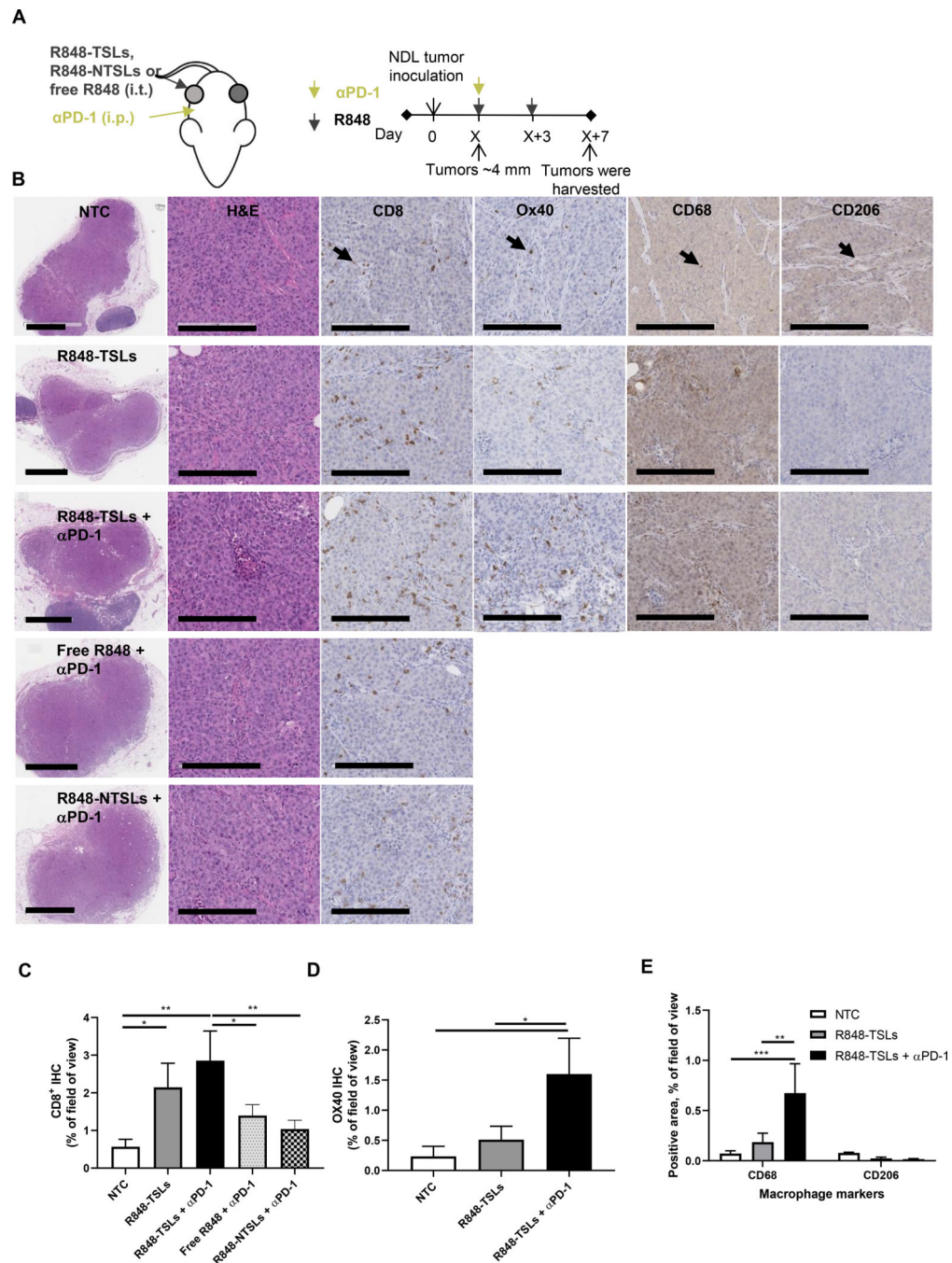
Figure 3.

Local injection of R848-TSLs, in combination with systemic αPD-1, activates the immune system in directly-treated transplanted NDL tumors and increases CD8^{+}, OX40^{+}, and CD68^{+} cells. A) Treatment regimen. B) Typical immunohistology images of no treatment control (NTC, 1st row), R848-TSLs (2nd row), R848-TSLs + αPD-1 (3rd row), free R848 + αPD-1 (4th row), and R848-NTSLs + αPD-1 (5th row) treated tumors (n= 3 each group), with H&E (low magnification on 1st column, higher magnification on 2nd column), CD8 (3rd column), OX40 (4th column), CD68 (5th column), and CD206 (6th column) staining. C-E)

Area fraction of positive IHC in tumor for CD8 (C), OX40 (D), CD68 and CD206 (E) expression. The scale bars in the low-magnification H&E images are 2 mm, and in other images are 200 μm. Black arrows indicate examples of positive cells. One-way ANOVA applied for C, D, two-way ANOVA for E. * $p < 0.05$; **$p < 0.01$; ***$p < 0.001$.
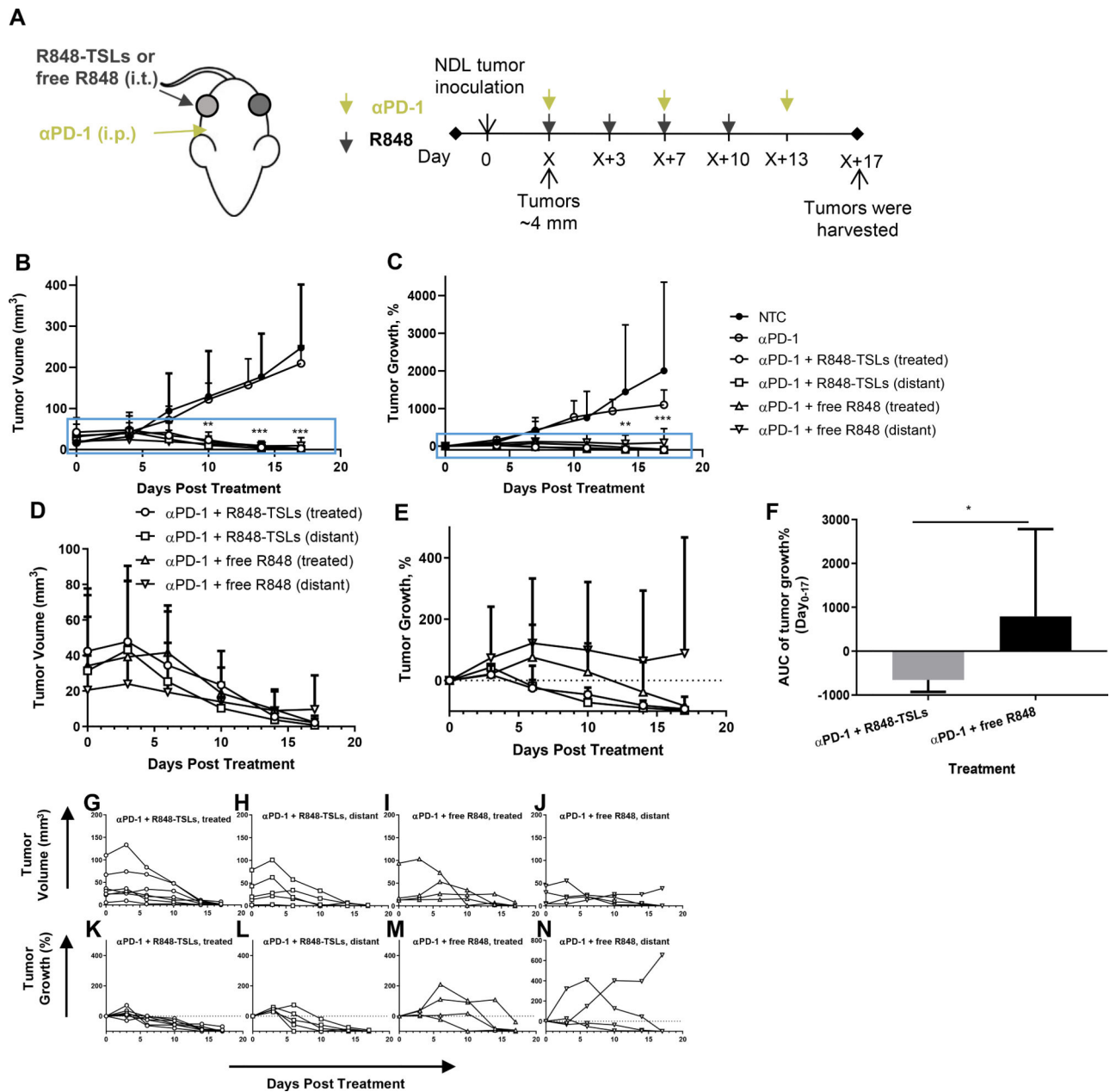
Figure 4.
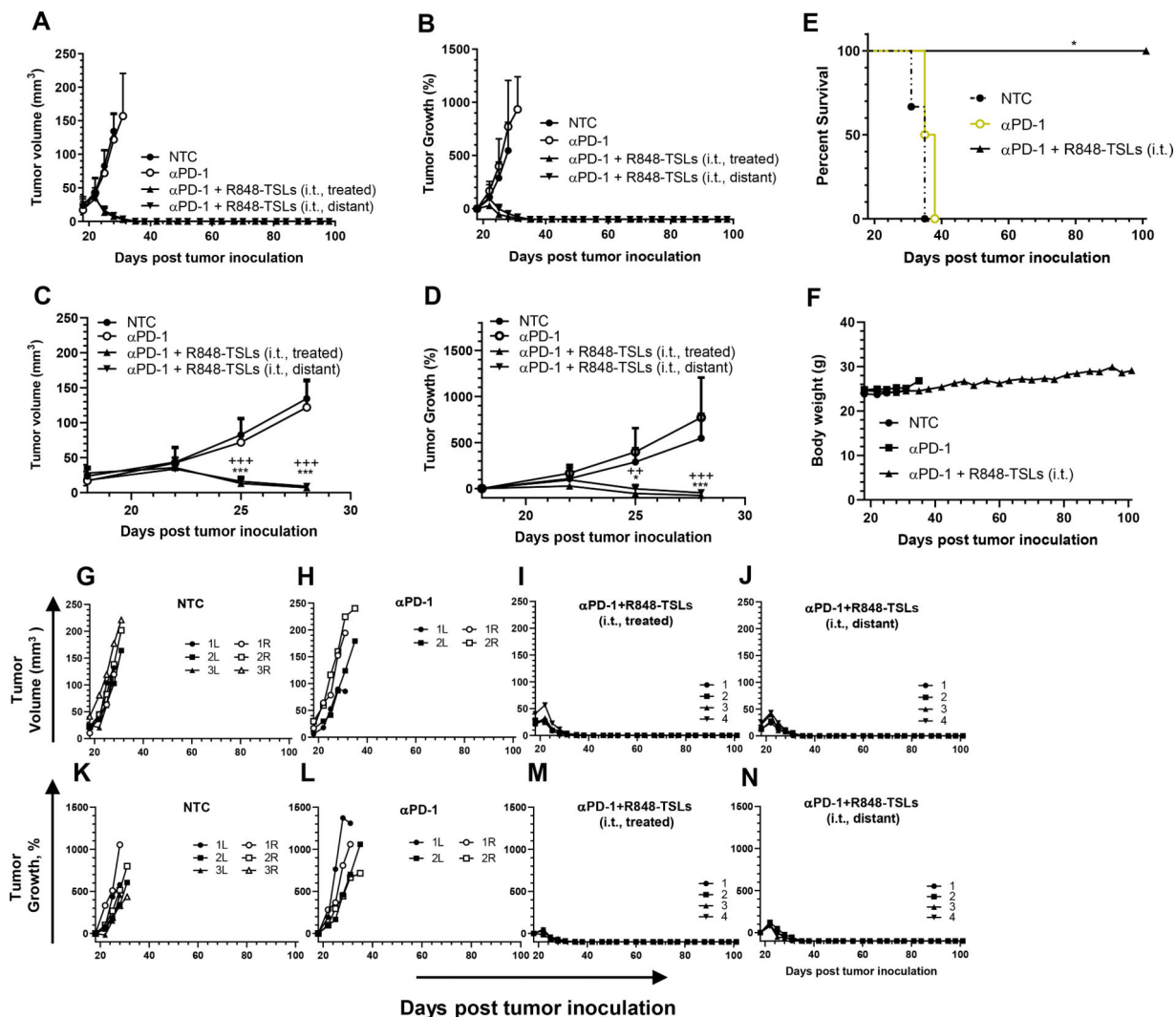Local injection of R848-TSLs regresses transplanted NDL tumors. A) Treatment regimen.
B, C) Tumor volumes (B) and tumor growth (C) of the non- treatment control (NTC, n = 5),
αPD-1 alone (n = 4), R848-TSLs with αPD-1 (n = 7) and free R848 with αPD-1 (n = 4)
treated and distant tumors. D, E) Magnified tumor volumes (D) and tumor growth (E) from
the magnified-boxes in B, C of R848-TSL and free R848-treated tumors, each combined
with αPD-1 treatment. F) Tumor growth area under the curve for R848-TSL and free R848-
treated mice over 0-–17 days of treatment. G-N) Tumor volume (G-J) and tumor growth (K-
N) for each tumor in the groups of R848-TSL treated (G, K), R848-TSL distant (H, L), free
R848 treated (I, M), and free R848 distant (J, N). "*", compared with NTC. One-way
ANOVA applied for B, C. * $p < 0.05$; **$p < 0.01$; ***$p < 0.001$.
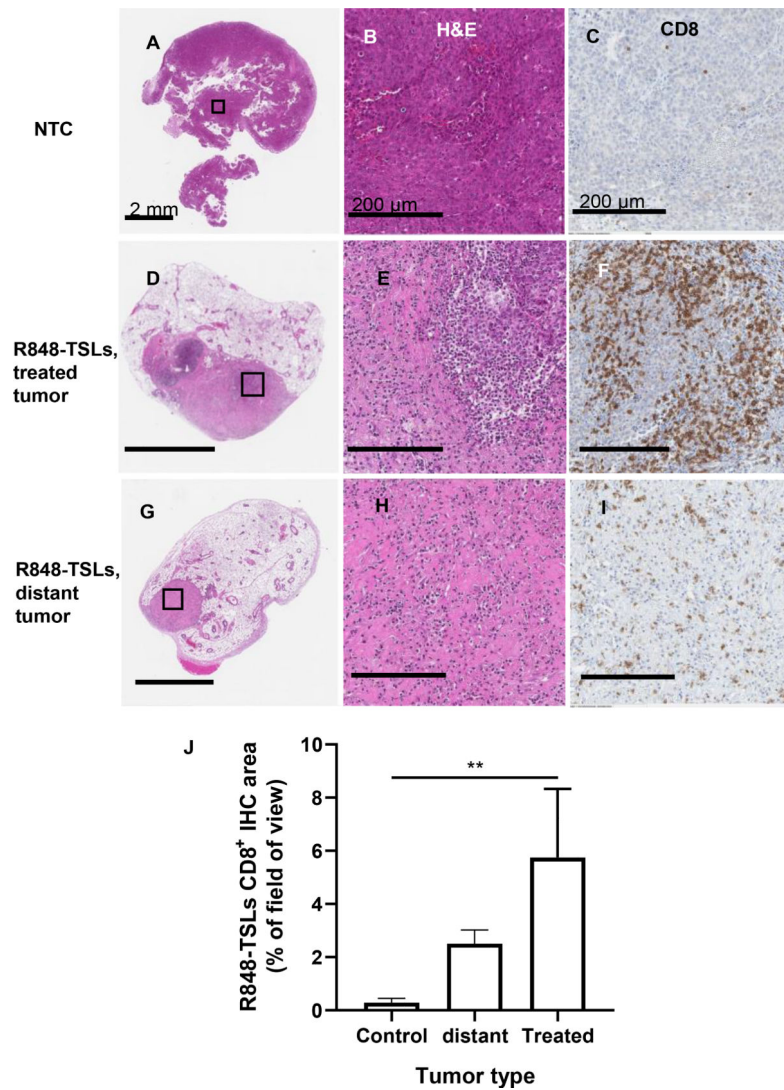
Figure 5.
For the treatment plan depicted in Fig. 4A, typical histology images of non-treatment-control (A-C), R848-TSL treated (D-F) and distant (G-I), tumors. H&E images with lower (A, D, G) and higher (B, E, H) magnifications. CD8 antibody-stained images (C, F, I) and CD8 area quantification in tumors (J). Mice received 4 injections of R848-TSLs and 3 injections of αPD-1 in total. The scale bars on the lower magnification images are 2 mm, and the scale bars on the higher magnification images are 200 μm. **, $p < 0.01$.

Figure 6.
With the treatment plan depicted in Fig. 4A, i.t. injection of R848-TSLs resulted in complete regression in an NDL tumor transplantation model: A-D) tumor volume (A, C), and tumor growth (B, D) for the entire period (A, B), magnified for the early days, (C, D); E) survival plot; F, body weights of the mice; G-N) the tumor volume (G-J) and growth (K-N) of each tumor in the groups of NTC (G, K), αPD-1 (H, L), αPD-1 + R848-TSLs i.t. treated (I, M), and αPD-1 + R848-TSLs i.t. distant (J, N), "*", compared with NTC; "+", compared with αPD-1; * p < 0.05; **p < 0.01; ***p < 0.001.
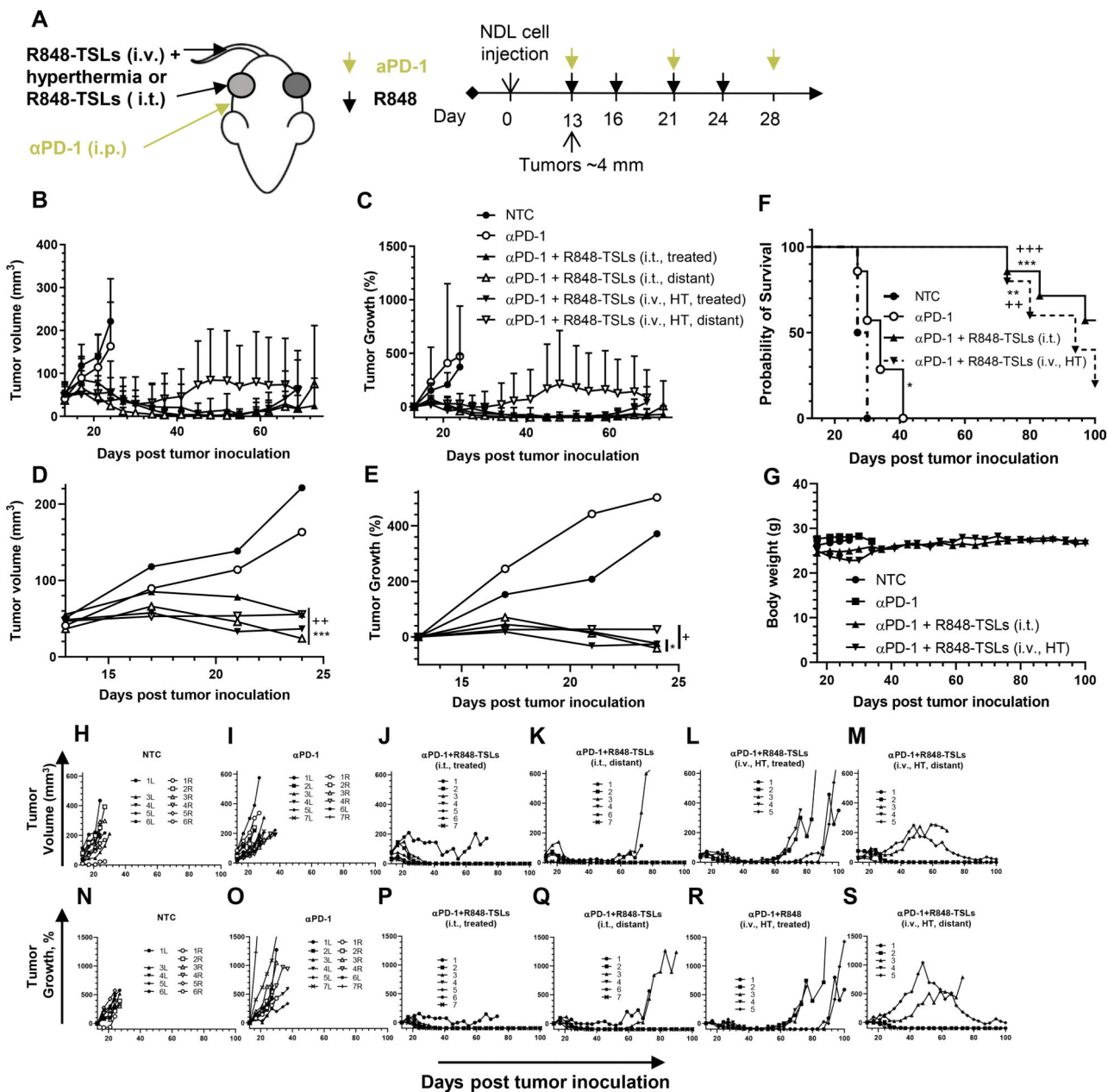
Figure 7.
With the treatment protocol depicted in Fig. 7A, i.t. or i.v. injections of R848-TSLs combined with hyperthermia delayed tumor growth and increased survival of mice with NDL tumors injected in the mammary fat pads. A) Treatment regimen, hyperthermia was applied to one tumor followed by R848-TSL injection i.v. B-E) Tumor volume (B, D) and tumor growth (C, E) for 100 days (B, C) and 28 days after tumor inoculation (D, E). F) Survival plot. G) Body weights over the survival study. H-S) Tumor volume (H-M) and growth (N-S) of each tumor in the NTC (H, N), αPD-1 (I, O), αPD-1+R848-TSLs i.t. treated (J, P), αPD-1 + R848-TSLs i.t. distant (K, Q), αPD-1 + R848-TSLs i.v.+ HT treated (L, R), and αPD-1+R848-TSLs i.v.+ HT distant cohorts (M, S). "*", compared with NTC;

"+", compared with αPD-1. One-way ANOVA applied for B, C. * p<0.05; **p<0.01; ***p<0.001.
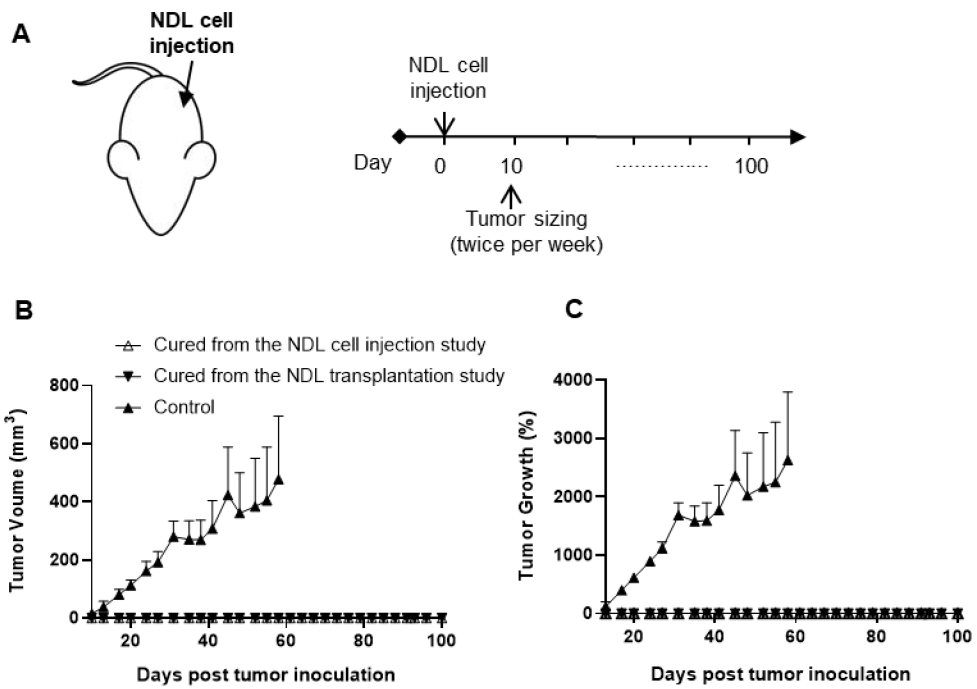
Figure 8.
Re-challenge study following treatment with αPD-1 + R848-TSLs (i.t.). A) Tumor monitoring plan. B) Tumor size. C) Tumor growth. Age-matched naive mice were studied as the control group. Data points represent the mean ± SEM (n = 4).

Table 1.

Trapping agents used for R848 loading.

Formulation	Trapping agent	External loading buffer
DPPC/DSPC/DSPC-PEG2K (85/10/5, mol%)	Ammonium sulfate Ammonium citrate Aluminum sulfate Copper sulfate Iron (II) sulfate	PBS –/– buffer (pH 7.4)

Table 2.

Animal grouping information for survival studies

	NTC	αPD-1	αPD-1 + i.t. R848-TSLs	αPD-1 + i.v. R848-TSLs + HT	Total
Transplanted tumor mice	3	3	4	0	10
Cell-injection tumor mice	6	7	7	5	25

Table 3.

Particle size and zeta potential of the empty liposomes and R848-TSLs. R848 was loaded remotely in TSLs via a 100 mM $FeSO_4$ loading gradient. D/L represents drug to lipid ratio. Data = mean ± SD ($n = 3$).

	Empty liposome	R848-TSLs
Diameter (nm)	107.1 ± 33.5	110.3 ± 19.8
PDI	0.098	0.032
D/L (w/w)	-	0.09 ± 0.01
Zeta Potential (mv)	−20.3 ± 13.6	−21.3 ± 10.9

Table 4.

Pharmacokinetic parameters of free R848 and R848-TSLs injected i.v. in FVB mice. C_{max}: maximum plasma concentration. $t_{1/2}$: half-life. $AUC_{0-\infty}$: area under the curve. Vd: volume of distribution Cl: clearance.

	C_{max} (µg/ml)	$t_{1/2}$ (h)	$AUC_{0-\infty}$ (µg/ml*h)	Vd (mL)	Cl (mL/h)
Free R848	2.61 ± 0.21	0.20 ± 0.05	0.63 ± 0.10	55.04 ± 6.39	195.06 ± 33.41
R848-TSLs	23.62 ± 1.13	0.53 ± 0.03	13.12 ± 0.67	7.07 ± 0.59	9.17 ± 0.48